

# Variational nonadiabatic dynamics in the moving crude adiabatic representation: Further merging of nuclear dynamics and electronic structure

Loïc Joubert-Doriot<sup>1</sup> and Artur F. Izmaylov<sup>1</sup>

*Department of Physical and Environmental Sciences, University of Toronto Scarborough, Toronto, Ontario, M1C 1A4, Canada; and Chemical Physics Theory Group, Department of Chemistry, University of Toronto, Toronto, Ontario, M5S 3H6, Canada*

(Dated: 3 October 2018)

A new methodology of simulating nonadiabatic dynamics using frozen-width Gaussian wavepackets within the moving crude adiabatic representation with the on-the-fly evaluation of electronic structure is presented. The main feature of the new approach is elimination of any global or local model representation of electronic potential energy surfaces, instead, the electron-nuclear interaction is treated explicitly using the Gaussian integration. As a result, the new scheme does not introduce any uncontrolled approximations. The employed variational principle ensures the energy conservation and leaves the number of electronic and nuclear basis functions as the only parameter determining the accuracy. To assess performance of the approach, a two-dimensional model with single electron and nuclear coordinates containing conical intersections between potential energy surfaces has been considered. Dynamical features associated with nonadiabatic transitions and nontrivial geometric (or Berry) phases were successfully reproduced within a limited basis expansion.

## I. INTRODUCTION

One of the popular approaches for on-the-fly simulations of quantum nonadiabatic dynamics involves representing the total molecular wavepacket as a Born-Huang expansion<sup>1,2</sup>

$$|\Psi(\mathbf{R}, t)\rangle = \sum_{s=1}^{N_s} \left[ \sum_{k=1}^{N_g} C_{ks}(t) g_k(\mathbf{R}, t) \right] |\phi_s(\mathbf{R})\rangle \quad (1)$$

using a linear combination of  $N_g$  moving frozen-width Gaussians  $g_k(\mathbf{R}, t)$  multiplied by  $N_s$  adiabatic electronic states  $|\phi_s(\mathbf{R})\rangle$ . Here,  $C_{ks}(t)$  are time-dependent coefficients, and  $\mathbf{R}$  are the nuclear coordinates. The states  $|\phi_s(\mathbf{R})\rangle$  are eigenstates of the electronic Hamiltonian  $\hat{H}_e[\mathbf{R}]$  and come naturally from well-developed electronic structure software packages. Unfortunately, commonly encountered conical intersections (CIs) of potential energy surfaces<sup>3,4</sup> produce two serious difficulties for fully quantum nonadiabatic methods in the adiabatic representation: 1) divergent nonadiabatic couplings from the nuclear kinetic operator acting on the electronic functions,<sup>5-7</sup> and 2) nontrivial geometric phases (GPs).<sup>8-11</sup>

To avoid these problems one can resort to the diabatic representation,<sup>12,13</sup> however, this would require extra system dependent work, diabaticization, which becomes an additional source of approximations.<sup>14</sup> Recently, we discovered that the problems of the adiabatic representation can be resolved without abandoning the direct use of the eigenfunctions of the electronic Hamiltonian.<sup>15</sup> The only required modification is to consider the adiabatic wavefunctions parametrically dependent on the center of moving nuclear wave-packets

$$|\Psi(\mathbf{R}, t)\rangle = \sum_{s=1}^{N_s} \sum_{k=1}^{N_g} C_{ks}(t) g_k(\mathbf{R}, t) |\phi_s(\mathbf{q}_k)\rangle, \quad (2)$$

where  $\mathbf{q}_k$  is the center of the  $g_k(\mathbf{R}, t)$  Gaussian. As illustrated on a two-state linear vibronic coupling model containing a CI,<sup>15</sup> due to absence of the nuclear coordinate dependence in the adiabatic electronic wavefunctions, both problems of the expansion in Eq. (1) are resolved: 1) the nuclear kinetic energy does not produce nonadiabatic couplings at all, and 2) the nontrivial GP is acquired naturally by the electronic wavefunctions due to their parametric dependence on Gaussian centers. We refer to the expansion in Eq. (2) as the moving crude adiabatic (MCA) representation. Independently, the same representation has been suggested by Shalashilin and coworkers under the name of time-dependent diabatic representation.<sup>16</sup> To use the MCA representation with electronic structure methods one needs to address challenges related to evaluation of new matrix elements originating from non-orthogonality of electronic wavefunctions centered at different Gaussians ( $\langle \phi_s(\mathbf{q}_k) | \phi_{s'}(\mathbf{q}_l) \rangle \neq \delta_{ss'}$  if  $\mathbf{q}_k \neq \mathbf{q}_l$ ) and from their non-eigenfunction character for the electronic Hamiltonian taken at an arbitrary nuclear point,  $H_e[\mathbf{R}]$ . In Refs. 16 and 17 evaluation of these new matrix elements was done using Taylor series expansions around the Gaussian centers. Although making implementation of the formalism feasible, such expansions introduce uncontrolled approximations whose quality depends on how strong is the nuclear dependence in solutions of the electronic problem, electronic wavefunctions and potential energy surfaces (PESs).

In the current work we show that the MCA representation can be used without introducing PESs and their local or global approximations. In this exact version, eMCA, the electronic states are calculated on-the-fly by solving the electronic problem first, and all the total Hamiltonian matrix elements in the MCA basis are then calculated exactly along molecular dynamics. eMCA assessment is done on a 2-dimensional generalization of the Shin and Metiu model,<sup>18</sup> which contains CIs and

exhibits coupled electron-nuclei dynamics. This model contains an explicit electron coordinate and therefore requires solving the electronic problem along with the nuclear dynamics.

In principle, the frozen-width Gaussians employed in Eqs. (1) and (2) can be evolved in several different ways: classically, using Born-Oppenheimer<sup>1,19</sup> or Ehrenfest trajectories,<sup>2,20</sup> or according to the time-dependent variational principle (TDVP) in a full quantum fashion.<sup>12,21–23</sup> We choose to apply the TDVP because its variational character accelerates the convergence of results with the number of basis functions.<sup>22</sup> Moreover, the energy is conserved by construction during the dynamics for variational equations of motion (EOM)<sup>24</sup>. In contrast, if classical EOM are used, the energy is conserved only in the complete basis set limit.<sup>25</sup>

The paper is organized as follows. Section II presents the formalism for the variational full quantum method using the MCA representation and discusses the new quantities needed for eMCA. In Sec. III, we explore the feasibility of eMCA on a realistic system where electronic and nuclear degrees of freedom (DOF) are treated explicitly for the on-the-fly dynamics. Finally, in Sec. IV we summarize main results and give future outlook.

## II. THEORY

### A. TDVP for MCA

Before applying TDVP in the MCA representation we will establish some additional notation and few useful relations for the nuclear basis functions expanded as frozen-width Gaussians

$$\langle \mathbf{R} | g_k(\mathbf{z}_k(t), \mathbf{z}_k(t)^*) \rangle = \prod_{a=1}^{N_n} \left( \frac{\omega_a}{\pi} \right)^{\frac{D}{4}} G_{ka}(\vec{R}_a), \quad (3)$$

$$G_{ka}(\vec{R}_a) = \prod_{\alpha=1}^D e^{-\frac{\omega_a}{2} [R_{a\alpha} - \sqrt{\frac{2}{\omega_a}} z_{ka\alpha}]^2 + i z_{ka\alpha} \text{Im}[z_{ka\alpha}]}, \quad (4)$$

where  $\mathcal{D}$  is the dimensionality of the space where particles are evolving (3-dimensional for real molecules) and  $\{\omega_a\}$  are the width parameters to be chosen for each nucleus.<sup>26</sup> The complex parameters  $z_{ka\alpha}$  encode the positions  $q_{ka\alpha}(t) = \sqrt{2/\omega_a} \text{Re}[z_{ka\alpha}(t)]$  and the momenta  $p_{ka\alpha}(t) = \sqrt{2\omega_a} \text{Im}[z_{ka\alpha}(t)]$  of each Gaussian. These relations stem from a coherent-state form of Gaussians introduced in Eq. (3)

$$\left[ \sqrt{\frac{\omega_a}{2}} \hat{R}_{a\alpha} + i \frac{\hat{P}_{a\alpha}}{\sqrt{2\omega_a}} \right] |g_k\rangle = z_{ka\alpha} |g_k\rangle, \quad (5)$$

where  $\hat{P}_{a\alpha}$  is the nuclear momentum operator. Use of coherent states is motivated by their numerical stability in the EOM integration.<sup>2,20,27</sup> Throughout this work, time and other parameters will be partially omitted from basis and state functions for readability. Also

we will use a shorthand notation for the MCA electronic states  $|\phi_s^k\rangle \equiv |\phi_s(\mathbf{q}_k)\rangle$  and for the electron-nuclear basis  $|\varphi_{ks}\rangle \equiv |g_k\rangle |\phi_s^k\rangle$ .

To solve the time-dependent Schrödinger equation for the full molecular Hamiltonian,  $\hat{H} = \hat{T}_n + \hat{H}_e[\mathbf{R}]$ , we apply the TDVP,<sup>28</sup> in the least action principle form

$$\text{Im} \langle \delta\Psi | \dot{\Psi} + i\hat{H}\Psi \rangle = 0, \quad (6)$$

where  $|\Psi\rangle$  is the molecular wavefunction given by Eq. (2). Due to non-analyticity of the MCA basis, different forms of the TDVPs are not generally equivalent.<sup>29</sup> Therefore, to ensure the energy conservation, it is important to apply the least action version of the TDVP. Then, the EOM for the parameters  $\{C_{ks}, z_{ka\alpha}\}$  become

$$i\dot{\mathbf{C}} = \mathbf{S}^{-1} [\mathbf{H} + i\boldsymbol{\gamma}] \mathbf{C}, \quad (7)$$

$$\mathbf{B}\dot{\mathbf{z}} + \mathbf{A}\dot{\mathbf{z}}^* = \mathbf{Y} + \bar{\mathbf{Y}}, \quad (8)$$

where the involved matrix elements can be written as

$$S_{kl,ss'} = \langle \varphi_{ks} | \varphi_{ls'} \rangle, \quad (9)$$

$$H_{kl,ss'} = \langle \varphi_{ks} | \hat{H} | \varphi_{ls'} \rangle, \quad (10)$$

$$\gamma_{kl,ss'} = \langle \varphi_{ks} | \dot{\varphi}_{ls'} \rangle, \quad (11)$$

$$Y_{ka\alpha} = i \sum_{lss'} C_{ks}^* \left\langle \frac{\partial \varphi_{ks}}{\partial z_{ka\alpha}} \left| \hat{1} - \hat{\mathcal{P}} \right| \hat{H} \varphi_{ls'} \right\rangle C_{ls'}, \quad (12)$$

$$\bar{Y}_{ka\alpha} = i \sum_{lss'} C_{ls'}^* \left\langle \hat{H} \varphi_{ls'} \left| \hat{1} - \hat{\mathcal{P}} \right| \frac{\partial \varphi_{ks}}{\partial z_{ka\alpha}^*} \right\rangle C_{ks}, \quad (13)$$

$$A_{kl,ab,\alpha\beta} = \sum_{ss'} \left[ C_{ls'}^* \left\langle \frac{\partial \varphi_{ls'}}{\partial z_{lb\beta}} \left| \hat{1} - \hat{\mathcal{P}} \right| \frac{\partial \varphi_{ks}}{\partial z_{ka\alpha}^*} \right\rangle C_{ks} - C_{ks}^* \left\langle \frac{\partial \varphi_{ks}}{\partial z_{ka\alpha}} \left| \hat{1} - \hat{\mathcal{P}} \right| \frac{\partial \varphi_{ls'}}{\partial z_{lb\beta}} \right\rangle C_{ls'} \right], \quad (14)$$

$$B_{kl,ab,\alpha\beta} = \sum_{ss'} \left[ C_{ls'}^* \left\langle \frac{\partial \varphi_{ls'}}{\partial z_{lb\beta}^*} \left| \hat{1} - \hat{\mathcal{P}} \right| \frac{\partial \varphi_{ks}}{\partial z_{ka\alpha}^*} \right\rangle C_{ks} - C_{ks}^* \left\langle \frac{\partial \varphi_{ks}}{\partial z_{ka\alpha}} \left| \hat{1} - \hat{\mathcal{P}} \right| \frac{\partial \varphi_{ls'}}{\partial z_{lb\beta}} \right\rangle C_{ls'} \right]. \quad (15)$$

Equations (12–15) involve the projector on the non-orthogonal basis

$$\hat{\mathcal{P}} = \sum_{kl,ss'} |\varphi_{ks}\rangle [\mathbf{S}^{-1}]_{kl,ss'} \langle \varphi_{ls'}|. \quad (16)$$

When the basis  $\{|\varphi_{ks}\rangle\}$  approaches the complete basis set limit,  $\hat{1} - \hat{\mathcal{P}}$  vanishes and eliminates Eq. (8) by turning it into the trivial identity,  $0 = 0$ . This illustrates that there is no need for basis function movement in the complete basis set limit.

In a more common case of an incomplete basis set, Eq. (8) can be combined with its complex conjugate equivalent and reformulated in a matrix form

$$\begin{pmatrix} \mathbf{Y} + \bar{\mathbf{Y}} \\ -\mathbf{Y}^* - \bar{\mathbf{Y}}^* \end{pmatrix} = \begin{pmatrix} \mathbf{B} & \mathbf{A} \\ \mathbf{A}^\dagger & -\mathbf{B}^T \end{pmatrix} \begin{pmatrix} \dot{\mathbf{z}} \\ \dot{\mathbf{z}}^* \end{pmatrix}. \quad (17)$$

This system of equations is solved as follows

$$\begin{pmatrix} \dot{z} \\ \dot{z}^* \end{pmatrix} = \begin{pmatrix} \beta & \alpha \\ \alpha^\dagger & -\beta^T \end{pmatrix} \begin{pmatrix} \mathbf{Y} + \bar{\mathbf{Y}} \\ -\mathbf{Y}^* - \bar{\mathbf{Y}}^* \end{pmatrix}, \quad (18)$$

where

$$\beta = \left[ \mathbf{B} + \mathbf{A} (\mathbf{B}^T)^{-1} \mathbf{A}^\dagger \right]^{-1} \quad (19)$$

$$\alpha = \mathbf{B}^{-1} \mathbf{A} \beta^T = \beta \mathbf{A} (\mathbf{B}^T)^{-1}. \quad (20)$$

It is important to note that  $\mathbf{A}$  and  $\alpha$  are antisymmetric, and  $\mathbf{B}$  and  $\beta$  are Hermitian.

The system energy is conserved by construction, as it can be verified by using Eq. (7), and then expressing the energy variation in terms of Eqs. (12), (13), and (18):

$$\begin{aligned} \dot{E} &= 2 \operatorname{Re} \langle \dot{\Psi} | \hat{H} | \Psi \rangle \\ &= 2 \operatorname{Re} \left[ i \bar{\mathbf{Y}}^\dagger \dot{z} - i \mathbf{Y}^T \dot{z}^* \right] \\ &= 2 \operatorname{Im} \left[ \begin{pmatrix} \bar{\mathbf{Y}} \\ -\mathbf{Y}^* \end{pmatrix}^\dagger \begin{pmatrix} \beta & \alpha \\ \alpha^\dagger & -\beta^T \end{pmatrix} \begin{pmatrix} \mathbf{Y} + \bar{\mathbf{Y}} \\ -\mathbf{Y}^* - \bar{\mathbf{Y}}^* \end{pmatrix} \right], \\ &= -2 \operatorname{Im} \left[ \begin{pmatrix} \bar{\mathbf{Y}}^* \\ -\mathbf{Y} \end{pmatrix}^T \begin{pmatrix} \alpha & \beta \\ -\beta^T & \alpha^\dagger \end{pmatrix} \begin{pmatrix} \bar{\mathbf{Y}}^* \\ -\mathbf{Y} \end{pmatrix} \right] = 0. \end{aligned} \quad (21)$$

In the last two equalities we used that  $\beta$  and  $\alpha$  are Hermitian and antisymmetric.

As illustrated next, all integrals defined in Eqs. (9)-(15) can be evaluated numerically exactly for the molecular Hamiltonian  $\hat{H}$ , and thus, the current formalism propagates Eqs. (7) and (8) numerically exactly within a finite basis set.

## B. Matrix elements

The matrix elements in Eq. (9) involves the product of the nuclear Gaussian overlap with overlap between electronic states obtained at different Gaussian centers

$$\begin{aligned} S_{kl,ss'} &= \langle g_k | g_l \rangle \langle \phi_s^k | \phi_{s'}^l \rangle \\ &= \exp \left[ \mathbf{z}_k^\dagger \mathbf{z}_l - \frac{|\mathbf{z}_k|^2 + |\mathbf{z}_l|^2}{2} \right] \langle \phi_s^k | \phi_{s'}^l \rangle. \end{aligned} \quad (22)$$

While the nuclear part has a simple analytic expression, the electronic part requires evaluating overlaps between states employing different primitive bases. Such electronic overlaps appear in other molecular dynamics methods, and therefore, have been already efficiently implemented.<sup>30</sup>

To treat the Hamiltonian integrals in Eq. (10), first, we added to and subtracted from the Hamiltonian the electron-nuclei ( $\hat{V}_{\text{en}}$ ) and nuclei-nuclei ( $\hat{V}_{\text{nn}}$ ) Coulomb terms evaluated at the center of a Gaussian so that we

can assemble the electronic Hamiltonian at the Gaussian center

$$\begin{aligned} \hat{H} &= \hat{T}_{\text{n}} + \hat{H}_e[\mathbf{R}] + (\hat{V}_{\text{en}}[\mathbf{q}] - \hat{V}_{\text{en}}[\mathbf{q}]) + (\hat{V}_{\text{nn}}[\mathbf{q}] - \hat{V}_{\text{nn}}[\mathbf{q}]) \\ &= \hat{T}_{\text{n}} + \hat{H}_e[\mathbf{q}] + (\hat{V}_{\text{en}}[\mathbf{R}] - \hat{V}_{\text{en}}[\mathbf{q}]) + (\hat{V}_{\text{nn}}[\mathbf{R}] - \hat{V}_{\text{nn}}[\mathbf{q}]). \end{aligned} \quad (23)$$

This allows us to reformulate the Hamiltonian integrals as

$$\begin{aligned} H_{kl,ss'} &= \langle \phi_s^k | \phi_{s'}^l \rangle \langle g_k | \hat{T}_{\text{n}} + \hat{V}_{\text{nn}}[\mathbf{R}] | g_l \rangle \\ &\quad + \langle \varphi_{ks} | \hat{V}_{\text{en}}[\mathbf{R}] - \hat{V}_{\text{en}}[\mathbf{q}_k] | \varphi_{ls'} \rangle \\ &\quad + \langle \varphi_{ks} | \varphi_{ls'} \rangle \left[ \epsilon_s(\mathbf{q}_k) - \hat{V}_{\text{nn}}[\mathbf{q}_k] \right], \end{aligned} \quad (24)$$

where  $\epsilon_s(\mathbf{q}_k)$  are the electronic energies at the point  $\mathbf{q}_k$ ,  $\hat{H}_e[\mathbf{q}_k] | \phi_s^k \rangle = \epsilon_s(\mathbf{q}_k) | \phi_s^k \rangle$ . The first term on the right-hand side of Eq. (24) can be easily calculated using Gaussian integration of the nuclear basis and overlap of the electronic states. The last term also requires the overlap of the basis functions as well as quantities that are known from electronic structure calculations. In contrast, the second term requires integration of  $\hat{V}_{\text{en}}$  over electronic states at different nuclear geometries. To evaluate it, we rewrite the second term as

$$\begin{aligned} \sum_{a,b=1}^{N_e, N_n} \left\langle \varphi_{ks} \left| \frac{Z_b}{|\vec{r}_a - \vec{R}_b|} - \frac{Z_b}{|\vec{r}_a - \vec{q}_{kb}|} \right| \varphi_{ls'} \right\rangle \\ = \int_{-\infty}^{\infty} d\vec{r} \rho_{ss'}^{kl}(\vec{r}) \bar{V}_{kl}(\vec{r}), \end{aligned} \quad (25)$$

where  $\{\vec{r}_a\}$  are the electronic positions,  $Z_b$  are the nuclear charges,  $\bar{V}_{kl}(\vec{r})$  is the electron-nuclei potential “dressed” by the Gaussian nuclear functions,

$$\begin{aligned} \bar{V}_{kl}(\vec{r}) &= \langle g_k | g_l \rangle \sum_b \frac{2Z_b}{\sqrt{\pi}} \left\{ \int_0^{\sqrt{\omega_b}} du e^{-u^2} \sum_{\alpha}^{\mathcal{D}} \left[ r_{\alpha} - \frac{z_{kb\alpha}^* + z_{lb\alpha}}{\sqrt{2\omega_b}} \right]^2 \right. \\ &\quad \left. - \int_0^{\infty} du e^{-u^2} \sum_{\alpha}^{\mathcal{D}} [r_{\alpha} - q_{kb\alpha}]^2 \right\}, \end{aligned} \quad (26)$$

and  $\rho_{ss'}^{kl}(\vec{r})$  is a “2-point” electronic transition density

$$\rho_{ss'}^{kl}(\vec{r}) = \sum_{ij} \chi_i^k(\vec{r})^* \chi_j^l(\vec{r}) \langle \phi_s^k | \hat{f}_i^{k\dagger} \hat{f}_j^l | \phi_{s'}^l \rangle. \quad (27)$$

Here,  $\hat{f}_i^{k\dagger}$  and  $\hat{f}_j^k$  are the creation and annihilation operators for the  $i^{\text{th}}$  molecular orbital,  $\chi_i^k(\vec{r})$ , used in the construction of the electronic states at  $\mathbf{q}_k$  (note that orbitals evaluated at  $\mathbf{q}_k$  and  $\mathbf{q}_l$  are not orthogonal with respect to each other). Transition densities between electronic states at different Gaussian centers require expansions in different primitive bases, which are obtained using nonunitary orbital transformations.<sup>31</sup>

The integrals involved in Eq. (11) can be expanded using the chain rule:

$$\begin{aligned} \gamma_{kl,ss'} = & \langle \phi_s^k | \phi_{s'}^l \rangle \left[ \left\langle g_k \left| \frac{\partial g_l}{\partial z_{l\alpha}} \right. \right\rangle \dot{z}_{l\alpha} + \left\langle g_k \left| \frac{\partial g_l}{\partial z_{l\alpha}^*} \right. \right\rangle \dot{z}_{l\alpha}^* \right] \\ & + \langle g_k | g_l \rangle \left\langle \phi_s^k \left| \frac{\partial \phi_{s'}^l}{\partial q_{l\alpha}} \right. \right\rangle \dot{q}_{l\alpha}. \end{aligned} \quad (28)$$

While the first two terms on the right-hand side can be calculated using coherent state properties and electronic overlaps, the last term involves a quantity that resembles the nonadiabatic couplings for MCA electronic states,  $\langle \phi_s^k | \partial \phi_{s'}^l / \partial q_{l\alpha} \rangle$ . Generally the number of electronic states considered in simulations can be too small to replace these terms by the expansion

$$\left\langle \phi_s^k \left| \frac{\partial \phi_{s'}^l}{\partial q_{l\alpha}} \right. \right\rangle = \sum_u \langle \phi_s^k | \phi_u^l \rangle \left\langle \phi_u^l \left| \frac{\partial \phi_{s'}^l}{\partial q_{l\alpha}} \right. \right\rangle \quad (29)$$

assuming the completeness of the electronic basis set. The exact calculation of the left hand side of Eq. (29) requires solving the coupled-perturbed equation<sup>32</sup>

$$\left[ \epsilon_s(\mathbf{q}_k) - \hat{H}_e[\mathbf{q}_k] \right] \left| \frac{\partial \phi_s^k}{\partial q_{k\alpha}} \right\rangle = \left[ \frac{\partial \hat{H}_e[\mathbf{q}_k]}{\partial q_{k\alpha}} - \frac{\partial \epsilon_s(\mathbf{q}_k)}{\partial q_{k\alpha}} \right] | \phi_s^k \rangle \quad (30)$$

Solving Eq. (30) is usual practice for energy gradients or derivative couplings by projecting analogues of Eq. (30) onto the electronic basis. A similar projection technique with the MCA electronic basis was used in the current work for solving Eq. (30).

Matrix elements in Eq. (12) to Eq. (15) contain integrals,

$$\begin{aligned} & \left\langle \frac{\partial \phi_s^k}{\partial q_{k\alpha}} \left| \frac{\partial \phi_{s'}^l}{\partial q_{l\beta}} \right. \right\rangle, \left\langle g_k \frac{\partial \phi_s^k}{\partial q_{k\alpha}} \left| \hat{H} \right| g_l \phi_{s'}^l \right\rangle, \\ & \text{and} \left\langle g_k \phi_s^k \left| \frac{\partial \hat{H}_e[\mathbf{R}]}{\partial R_{a\alpha}} \right| g_l \phi_{s'}^l \right\rangle, \end{aligned} \quad (31)$$

which are implemented using components obtained earlier in this section. Note that these integrals are required for the EOM obtained employing fully quantum consideration, if the basis set dynamic is replaced by classical<sup>19</sup> or Ehrenfest dynamics<sup>20</sup> these integrals do not appear.

Thus, the new quantities for which calculations are not already available in electronic structure calculation packages are: the ‘‘2-point’’ electronic transition densities given in Eq. (27), and the ‘‘2-point’’ electronic states overlap derivatives appearing in Eq. (29). These two quantities are also the most computationally intense parts of the current approach. They appear in the integrals Eq. (10) and Eq. (11), whose number scale quadratically with the number of basis functions. However, the nuclear functions’ overlap, which is an exponentially decaying function with respect to differences between the Gaussian parameters, appears in both integrals and can be used for efficient screening<sup>33</sup> to reduce the scaling to linear.

### C. Adiabatic nuclear densities

While the MCA representation aims to avoid constructing the global adiabatic representation during the simulations, one may still want to analyze the results in terms of quantities projected onto the global adiabatic representation. This can be done straightforwardly if the projector onto an adiabatic state,  $\hat{Q}_n[\mathbf{R}] = |\phi_n(\mathbf{R})\rangle \langle \phi_n(\mathbf{R})|$ , is available. Here, we describe a construction of an approximate projection to a  $n^{\text{th}}$  adiabatic state. As a quantity of interest we consider the adiabatic nuclear density

$$\rho_n(\mathbf{R}) = \left\langle \Psi(\mathbf{R}) \left| \hat{Q}_n[\mathbf{R}] \right| \Psi(\mathbf{R}) \right\rangle. \quad (32)$$

One obvious approximation of  $\hat{Q}_n[\mathbf{R}]$  can be its first-order Taylor series expansion around a particular Gaussian center

$$\begin{aligned} \hat{Q}_n[\mathbf{R}] & \approx \hat{Q}_n^{(1)}|_{\mathbf{q}_k} \\ & = \hat{Q}_n[\mathbf{q}_k] + \sum_{a\alpha} \frac{\partial \hat{Q}_n}{\partial R_{a\alpha}} \Big|_{\mathbf{q}_k} (R_{a\alpha} - q_{ka\alpha}). \end{aligned} \quad (33)$$

However, the choice of the expansion center can be non-trivial considering that  $|\Psi(\mathbf{R})\rangle$  is expanded using a linear combination of Gaussians located in different places. A special care is required in the case of cross-terms, where differently centered Gaussians are originating from  $\langle \Psi(\mathbf{R})|$  and  $|\Psi(\mathbf{R})\rangle$ . One may suggest a double-centered expansion for the  $\hat{Q}_n[\mathbf{R}]$ . It turns out that the double-centered expansion does not only violate the idempotency but also can introduce spurious double-valuedness in cases with CIs. In what follows we adhere to a particular choice that on the one hand provides accurate expansion tailored to individual terms in  $\langle \Psi(\mathbf{R})|$  and  $|\Psi(\mathbf{R})\rangle$ , and on the other hand conserves the correct topological properties of  $\rho_n(\mathbf{R})$  associated with GP. Using the idempotency of the projector operator we rewrite the density as

$$\begin{aligned} \rho_n(\mathbf{R}) & = \left\langle \Psi(\mathbf{R}) \left| \hat{Q}_n[\mathbf{R}] \hat{Q}_n[\mathbf{R}] \right| \Psi(\mathbf{R}) \right\rangle \quad (34) \\ & = \left\| \sum_{ks} \hat{Q}_n[\mathbf{R}] | \phi_s^k \rangle g_k(\mathbf{R}) C_{ks} \right\|^2. \end{aligned} \quad (35)$$

Then, each  $\hat{Q}_n[\mathbf{R}] | \phi_s^k \rangle$  term is substituted by the first-order approximation centered at the Gaussian center  $\mathbf{q}_k$ , which gives

$$\begin{aligned} \rho_n(\mathbf{R}) & \approx \sum_{kl,ss'} C_{ks}^* C_{ls'} g_k(\mathbf{R})^* g_l(\mathbf{R}) \\ & \times \left\langle \phi_s^k \left| \hat{Q}_n^{(1)}|_{\mathbf{q}_k} \hat{Q}_n^{(1)}|_{\mathbf{q}_l} \right| \phi_{s'}^l \right\rangle. \end{aligned} \quad (36)$$

This approach has two more advantages:  $\rho_n(\mathbf{R})$  is positively definite and can be improved systematically by adding higher order terms in the Taylor expansion of

Eq. (33). The adiabatic population  $P_n^a$  is then calculated by integrating over the nuclear DOF

$$P_n^a \approx \int_{-\infty}^{\infty} d\mathbf{R} \rho_n(\mathbf{R}). \quad (37)$$

Since  $\rho_n(\mathbf{R})$  and  $P_n^a$  are approximated quantities, they do not add up to unity. To remedy this deficiency, both quantities are renormalized by  $\sum_n P_n^a$ .

#### D. Model

For numerical illustrations we use a two-dimensional ( $\mathcal{D} = 2$ ) generalization<sup>18</sup> of the model Hamiltonian introduced by Shin and Metiu.<sup>34,35</sup> This model contains three nuclei and one electron, the positions of two nuclei are fixed, which leaves one electron ( $\vec{r}$ ) and one nuclear ( $\vec{R}$ ) 2D coordinates to consider. The masses and the charges of the nuclei are  $M = 10$  and  $Z = 1$ , respectively. The Coulomb potential is replaced by a soft Coulomb potential, and the electronic Hamiltonian is

$$\begin{aligned} \hat{H}_e[\vec{R}] = & \sum_{\alpha} \frac{\hat{p}_{\alpha}^2}{2} + V(0.5; |\vec{r} - \vec{R}|) + V(0.5; |\vec{r} - \vec{R}_+|) \\ & + V(0.5; |\vec{r} - \vec{R}_-|) + V(10; |\vec{R} - \vec{R}_+|) \\ & + V(10; |\vec{R} - \vec{R}_-|) + V(10; L) + \left( \frac{|\vec{R}|}{3.5} \right)^4, \end{aligned} \quad (38)$$

where  $V(\Delta; x) = (\Delta + x^2)^{-1/2}$ ,  $L = 4\sqrt{3}/5$  a.u.,  $\vec{R}_{\pm} = (\pm L/2, 0)$  are the positions of the fixed protons, and the last term is the two-dimensional quartic potential to ensure the system is bounded. This electronic Hamiltonian gives rise to CIs (see Fig. 1) between the first ( $D_1$ ) and second ( $D_2$ ) adiabatic excited states.<sup>18,36</sup> Thus, this model represents a realistic test case for nonadiabatic simulations where on-the-fly quantum dynamics can be done exactly.

#### E. Numerical details

The eMCA method is tested by modeling nonadiabatic dynamics of a wavepacket prepared on the  $D_2$  electronic state

$$|\Psi(t=0, \mathbf{R})\rangle \propto e^{-\frac{\omega}{2}|\mathbf{R}-\mathbf{q}|^2} |\phi_2(\mathbf{q})\rangle. \quad (39)$$

where  $\mathbf{q} = (0, 2)$ . This initial position of the wavepacket is close to the CI between  $D_1$  and  $D_2$  electronic surfaces. To adequately represent dynamic of the wavepacket and to avoid numerical complications associated with the Gaussian center collision with the CI, the initial Gaussian is presented as a linear combination of four Gaussians with a smaller width corresponding to  $\omega = 6.818$ .

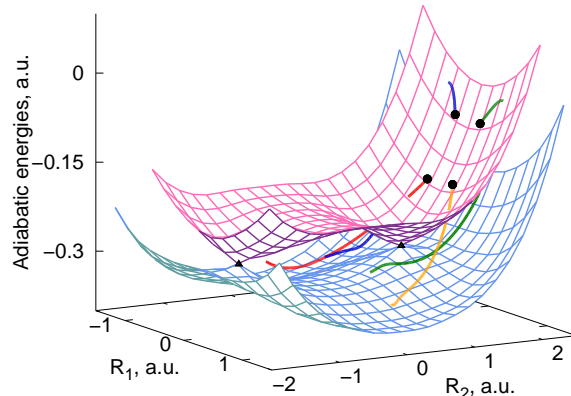


FIG. 1. Adiabatic potential energy surfaces for  $D_1$  (in blue) and  $D_2$  (in pink). Two symmetry allowed CIs are represented by the black triangles with coordinates  $(0.0, \pm 1.2)$ . The colored lines are trajectories of the Gaussian basis for the simulation with 4 Gaussian functions during the first 9 a.u. of time propagation for which black circles are initial positions.

The initial parameters for these Gaussians were chosen as  $C_{k3} = 0.287$  and  $C_{ks \neq 3} = 0$ , initial positions  $\mathbf{q}_k = (\pm 0.214, 2 \pm 0.205)$ , and zero initial momenta. The trajectories resulting from these initial conditions are shown in Fig. 1 and skirt the CI in a symmetric manner.

The electronic states are expanded in a direct product basis of harmonic oscillator eigenfunctions. This harmonic basis is centered at the electronic coordinate origin  $(0, 0)$  and is defined by its frequency, 0.327, chosen to be the same for both electronic dimensions. The number of the basis functions, maximum quanta, was also chosen the same for both dimensions,  $n_{x,\max} = n_{y,\max} = n_{\max} = 30$ . The total direct product basis containing 900 states has been pruned to 465 products for which  $n_x + n_y \leq n_{\max}$ .

Matrices  $\mathbf{S}$ ,  $\mathbf{B}$ , and  $\mathbf{B} + \mathbf{A}(\mathbf{B}^T)^{-1}\mathbf{A}^\dagger$  need to be inverted in order to solve Eq. (7) and Eq. (18). These matrices can be close to singular due to overcompleteness of the Gaussian basis for  $\mathbf{S}$ , and due to small populations  $C_{ks}^* C_{ls'}$  for  $\mathbf{B}$  and  $\mathbf{B} + \mathbf{A}(\mathbf{B}^T)^{-1}\mathbf{A}^\dagger$ . To avoid numerical difficulties, we used a regularization of the inversion procedure that replaces singular values  $\lambda \rightarrow \lambda + \varepsilon \exp(-\lambda/\varepsilon)$ , where  $\varepsilon$  is a threshold. Since the accuracy of the  $\mathbf{S}$  inversion is essential for the quantum propagation of Eq. (7), we use a very small threshold  $\varepsilon = 10^{-6}$  for this step. In contrast, solving Eq. (8) only gives an optimal evolution of the Gaussian basis but does not impact significantly the accuracy when a sufficient number of Gaussians is used. Thus, we use a larger threshold for Eq. (8),

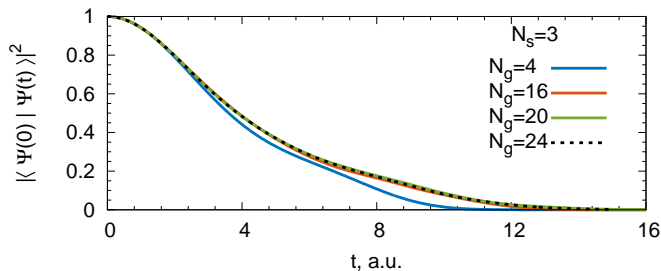


FIG. 2. Autocorrelation function norm  $|\langle \Psi(0) | \Psi(t) \rangle|^2$  for different number of Gaussian functions and  $N_s = 3$  MCA states.

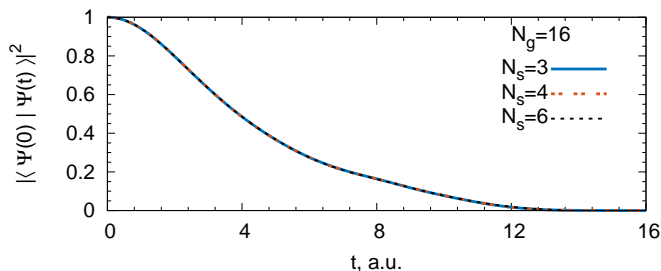


FIG. 3. Autocorrelation function norm  $|\langle \Psi(0) | \Psi(t) \rangle|^2$  for different number of MCA states and  $N_g = 16$  Gaussian functions. All lines are almost indistinguishable.

$\epsilon \leq 10^{-3}$ . All EOMs have been solved using the 4<sup>th</sup> order ode45 integrator implemented in the MATLAB program.<sup>37</sup>

### III. RESULTS AND DISCUSSION

First, we illustrate the convergence with respect to the basis size by comparing the norm of the autocorrelation function  $|\langle \Psi(0) | \Psi(t) \rangle|^2$  for different numbers of Gaussian functions in Fig. 2 and electronic states in Fig. 3. The convergence with respect to the latter is already achieved for  $N_s = 3$  (see Fig. 3) due to a large energy gap between a cluster of the first three states,  $D_{0-2}$ , and the rest (e.g., at the initial geometry,  $\epsilon_2 - \epsilon_1 = 0.106$  a.u. and  $\epsilon_3 - \epsilon_2 = 0.326$  a.u.).

Nonadiabatic dynamics is illustrated in Fig. 4 for the case of  $N_g = 4$  and  $N_s = 3$ . One of the main features of this dynamics is radiationless population transfer between adiabatic states, which takes place in the vicinity of the CI. Another feature is related to a nontrivial geometric (or Berry) phase induced by CIs between  $D_1$  and  $D_2$ , the nuclear density corresponding to an adiabatic state exhibits a nodal line upon skirting one CI,<sup>11,15,38</sup> this node disappears after encircling a second CI.<sup>39,40</sup> Since the wavepacket starts on  $D_2$  it must display a nodal line between the two CIs on  $D_2$  and the absence of the nodal line between the CIs on  $D_1$ . Indeed, these nodal features can be observed in our simulations with a nodal line appearing on  $D_1$  for  $1.2 < R_1 < -1.2$  [see Fig. 5-(a,c)] and

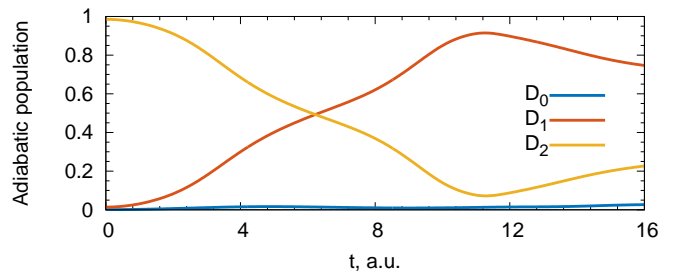


FIG. 4. Population of the three first adiabatic states for  $N_g = 4$  and  $N_s = 3$ .

on  $D_2$  for  $-1.2 < R_1 < 1.2$  [see Fig. 5-(b)].

Figures 5-(a-c) used the approximate expressions for the adiabatic nuclear densities derived in Eq. (36). We have also calculated the corresponding exact adiabatic densities on a grid by generating the exact adiabatic states at each point. The approximate and exact densities were found to be visually indistinguishable which confirms the quality of the employed approximation.

Deviation of the norm of the wavefunction as well as the relative energy deviation  $\langle \Psi | \hat{H} | \Psi \rangle / E_0$  ( $E_0$  is chosen as the energy difference of the adiabatic states  $D_1$  and  $D_2$  at the initial position) was smaller than  $10^{-5}$  in all our simulations. This number is the numerical precision of the current method considering the error introduced by the regularization to solve Eq. (7) and error accumulation along the propagation.

### IV. CONCLUSIONS

Using the 2D model with explicit electron and nuclear DOF we demonstrated feasibility of the eMCA approach for on-the-fly simulations of nonadiabatic dynamics without approximating the involved matrix elements. Owing to its capability for exact calculation of matrix elements, the eMCA approach provides a route to quantum dynamics with controlled approximations. eMCA is fully variational, which ensures the system energy conservation at any setup. The only parameter defining the accuracy of the eMCA approach is the basis set size. It was shown that the MCA expansion has a convergence with the number of explicitly included electronic states similar to what would be expected from the conventional Born-Huang expansion using the adiabatic electronic states. This can be rationalized considering that even though MCA involves crude adiabatic states their interactions due to nonorthogonality in different nuclear geometry points are attenuated by exponentially decaying overlaps of attached nuclear Gaussian functions. Systematic improvement of the MCA representation with respect to the number of nuclear Gaussian functions can be done using spawning<sup>19,41</sup> and cloning<sup>17,20,42</sup> approaches.

Implementing eMCA in conjunction with electronic structure methods will require the calculation of the electronic transition densities and electronic state overlap

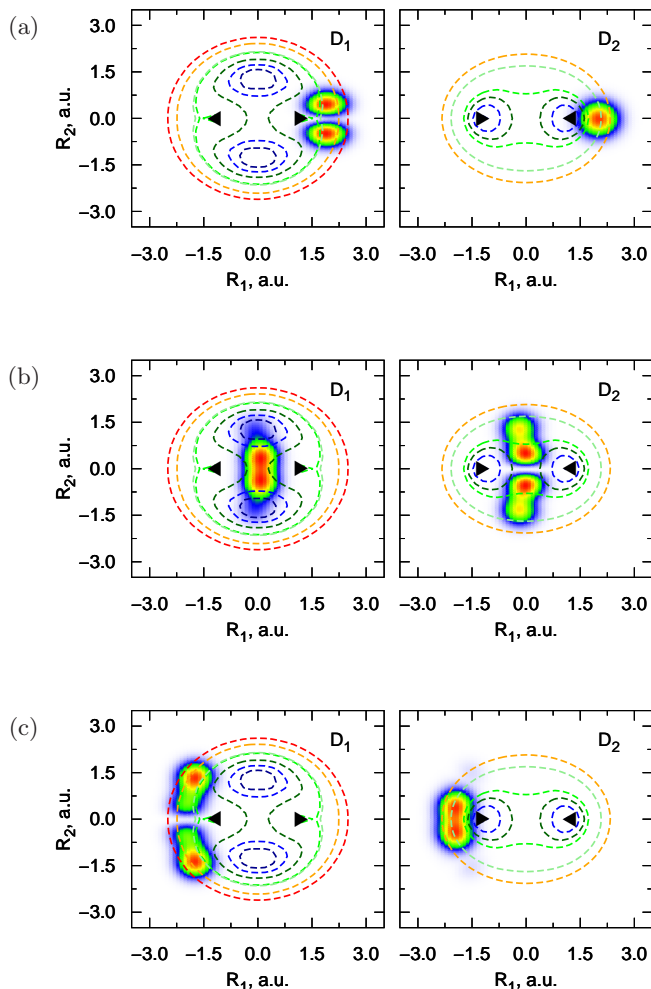


FIG. 5. Nuclear density of adiabatic states  $D_1$  (on the left) and  $D_2$  (on the right) at different time: (a)  $t = 0$ , (b)  $t = 13.9$ , (c)  $t = 26.2$ . Contours of the adiabatic potential energy surfaces of  $D_1$  and  $D_2$  are superimposed to the densities. Triangles indicate the CIs positions.

derivatives for different nuclear geometries. Electronic structure algorithms for finding these quantities with electronic functions at the same nuclear geometry are already available and can be extended for eMCA. Furthermore, eMCA can be extended to even larger system using quantum-classical treatment<sup>43</sup> or non-unitary dynamics combined with the system-environment partitioning.<sup>44</sup>

Finally, the explicit treatment of the electronic DOF will make eMCA a method of choice for studying the electronic dynamics on short timescales of femto- or sub-femtoseconds while treating the electron-nuclei interaction exactly. This interaction is essential for elucidating a role of the nuclear motion for electronic decoherence.<sup>45</sup>

## V. ACKNOWLEDGEMENTS

The authors thank Ilya Ryabinkin for helpful discussions. This work was supported by a Sloan Research Fellowship, Natural Sciences and Engineering Research Council of Canada (NSERC).

- <sup>1</sup>S. Yang, J. D. Coe, B. Kaduk, and T. J. Martínez, *J. Chem. Phys.* **130**, 134113 (2009).
- <sup>2</sup>K. Saita and D. V. Shalashilin, *J. Chem. Phys.* **137**, 22A506 (2012).
- <sup>3</sup>D. R. Yarkony, *Acc. Chem. Res.* **31**, 511 (1998).
- <sup>4</sup>A. Migani and M. Olivucci, in *Conical Intersection Electronic Structure, Dynamics and Spectroscopy*, edited by W. Domcke, D. R. Yarkony, and H. Köppel (World Scientific, New Jersey, 2004) p. 271.
- <sup>5</sup>G. A. Meek and B. G. Levine, *J. Chem. Phys.* **144**, 184109 (2016).
- <sup>6</sup>P. Saxe and D. R. Yarkony, *J. Chem. Phys.* **86**, 321 (1987).
- <sup>7</sup>T. C. Thompson, D. G. Truhlar, and C. A. Mead, *J. Chem. Phys.* **82**, 2392 (1985).
- <sup>8</sup>C. A. Mead and D. G. Truhlar, *J. Chem. Phys.* **70**, 2284 (1979).
- <sup>9</sup>C. A. Mead, *Rev. Mod. Phys.* **64**, 51 (1992).
- <sup>10</sup>C. Wittig, *Phys. Chem. Chem. Phys.* **14**, 6409 (2012).
- <sup>11</sup>I. G. Ryabinkin, L. Joubert-Doriol, and A. F. Izmaylov, *Acc. Chem. Res.* **50**, 1785 (2017).
- <sup>12</sup>G. A. Worth, M. A. Robb, and I. Burghardt, *Faraday Discuss.* **127**, 307 (2004).
- <sup>13</sup>G. A. Meek and B. G. Levine, *J. Chem. Phys.* **145**, 184103 (2016).
- <sup>14</sup>C. A. Mead and D. G. Truhlar, *J. Chem. Phys.* **77**, 6090 (1982).
- <sup>15</sup>L. Joubert-Doriol, J. Sivasubramanium, I. G. Ryabinkin, and A. F. Izmaylov, *J. Phys. Chem. Lett.* **8**, 452 (2017).
- <sup>16</sup>S. Fernandez-Alberti, D. V. Makhov, S. Tretiak, and D. V. Shalashilin, *Phys. Chem. Chem. Phys.* **18**, 10028 (2016).
- <sup>17</sup>D. V. Makhov, W. J. Glover, T. J. Martínez, and D. V. Shalashilin, *J. Chem. Phys.* **141**, 054110 (2014).
- <sup>18</sup>S. K. Min, A. Abedi, K. S. Kim, and E. Gross, *Phys. Rev. Lett.* **113**, 263004 (2014).
- <sup>19</sup>M. Ben-Nun and T. J. Martínez, *Adv. Chem. Phys.* **121**, 439 (2002).
- <sup>20</sup>D. V. Makhov, C. Symonds, S. Fernandez-Alberti, and D. V. Shalashilin, *Chem. Phys.* **493**, 200 (2017).
- <sup>21</sup>I. Burghardt, K. Giri, and G. A. Worth, *J. Chem. Phys.* **129**, 174104 (2008).
- <sup>22</sup>G. A. Worth, M. A. Robb, and B. Lasorne, *Mol. Phys.* **106**, 2077 (2008).
- <sup>23</sup>G. W. Richings and G. A. Worth, *Chem. Phys. Lett.* **683**, 606 (2017).
- <sup>24</sup>K.-K. Kan, *Phys. Rev. A* **24**, 2831 (1981).
- <sup>25</sup>S. Habershon, *J. Chem. Phys.* **136**, 014109 (2012).
- <sup>26</sup>A. L. Thompson, C. Punwong, and T. J. Martínez, *Chem. Phys.* **370**, 70 (2010).
- <sup>27</sup>A. F. Izmaylov, *J. Chem. Phys.* **138**, 104115 (2013).
- <sup>28</sup>P. Kramer and M. Saraceno, *Geometry of the Time-Dependent Variational Principle in Quantum Mechanics* (Springer, New York, 1981).
- <sup>29</sup>J. Broeckhove, L. Lathouwers, E. Kesteloot, and P. Van Leuven, *Chem. Phys. Lett.* **149**, 547 (1988).
- <sup>30</sup>F. Plasser, M. Ruckebauer, S. Mai, M. Oppel, P. Marquetand, and L. González, *J. Chem. Theory Comput.* **12**, 1207 (2016).
- <sup>31</sup>P. Å. Malmqvist, *Int. J. Quantum Chem.* **30**, 479 (1986).
- <sup>32</sup>Y. Osamura, *Theor. Chim. Acta* **76**, 113 (1989).
- <sup>33</sup>P. M. W. Gill, B. G. Johnson, and J. A. Pople, *Chem. Phys. Lett.* **217**, 65 (1994).
- <sup>34</sup>S. Shin and H. Metiu, *J. Chem. Phys.* **102**, 9285 (1995).
- <sup>35</sup>S. Shin and H. Metiu, *J. Phys. Chem.* **100**, 7867 (1996).
- <sup>36</sup>K. Hader, J. Albert, E. K. U. Gross, and V. Engel, *J. Chem. Phys.* **146**, 074304 (2017).
- <sup>37</sup>MATLAB, version 8.0.0.783 (R2012b). The MathWorks Inc., Natick, Massachusetts (2012).

- <sup>38</sup>J. Schön and H. Köppel, *J. Chem. Phys.* **103**, 9292 (1995).
- <sup>39</sup>J. W. Zwanziger and E. R. Grant, *J. Chem. Phys.* **87**, 2954 (1987).
- <sup>40</sup>W. Domcke and D. R. Yarkony, *Annu. Rev. Phys. Chem.* **63**, 325 (2012).
- <sup>41</sup>A. F. Izmaylov, *J. Chem. Phys.* **138**, 104115 (2013).
- <sup>42</sup>A. F. Izmaylov and L. Joubert-Doriol, *J. Phys. Chem. Lett.* **8**, 1793 (2017).
- <sup>43</sup>S. Römer and I. Burghardt, *Mol. Phys.* **111**, 3618 (2013).
- <sup>44</sup>L. Joubert-Doriol and A. F. Izmaylov, *J. Chem. Phys.* **142**, 134107 (2015).
- <sup>45</sup>M. Vacher, M. J. Bearpark, M. A. Robb, and J. P. Malhado, *Phys. Rev. Lett.* **118**, 083001 (2017).